Mechanics of tubular meshes made of helical fibers and application to modeling McKibben artificial muscles

Jacopo Quaglierini[1], Marino Arroyo[2] and Antonio DeSimone[3]

***Abstract*— McKibben artificial muscles are an important example of braided, tubular structures made of many interwoven helical fibers. Their highly non-linear response is very robust and reproducible, making them particularly suitable for applications in Soft Robotics. The rich behavior of McKibben actuators has been studied either through minimal geometric models or through complex Finite Elements Method (FEM) simulations. To obtain a simpler yet accurate model for McKibben actuators, we develop a simplified framework entirely based on the geometry of the virtual envelope surface defined by the fibers of the mesh. In the axisymmetric cases studied here, the problem boils down to solving for a single scalar field of one scalar variable. We validate our model by solving contractor and extensor muscle configurations and comparing them against experimental and numerical results from the literature, achieving good agreement at a significantly lower computational cost. Simulations reveal that loads are sustained mostly by the braided mesh, whereas the inner chamber stores most of the external work as elastic energy. This phenomenon explains why simplified formulas for force-pressure relationship may be quite effective in predicting the behavior of McKibben actuators.**

2023 IEEE International Conference on Soft Robotics (RoboSoft) | 979-8-3503-3222-3/23/$31.00 ©2023 IEEE | DOI: 10.1109/ROBOSOFT55895.2023.10122020

I. Introduction

Braided meshes used in McKibben artificial muscles are an important example of tubular structures made of many interwoven helical fibers [1, 2, 3]. These actuators are made of an elastomeric chamber, connected to an external air supply, surrounded by a cylindrical mesh of helical fibers clamped at its bases. The mesh transforms the radial expansion into axial displacement, so that it transduces a uniform input (pressure) into a directional output (displacement); depending on the braiding angle θ (see Fig. 2), under internal pressure the actuator increases its enclosed volume by contracting or elongating along its axis. Indeed, by neglecting boundary effects due to clamping, we can approximate the volume-angle relationship with that of a cylindrical mesh with free ends, shown in Fig. 1. The volume $V(\theta)$ has a maximum at $\theta = \theta^* = \arctan\left(1/\sqrt{2}\right) \approx 35°26'$, the so called "magic angle": at that point, an increase in pressure cannot cause any further increase in volume, but only a stiffening of the structure, and there is no change in θ. At smaller or larger angles, the increasing enclosed volume causes elongation (extensor behavior) or contraction (contractor behavior) of the actuator, respectively. Despite its high non-linearity, caused by the variation in geometry of the helical fibers, the elastic response of these soft pneumatic actuators is very robust and reproducible, making them particularly suitable for applications in Soft Robotics.

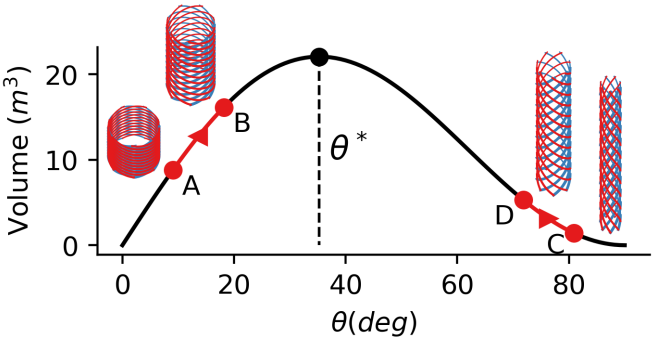

Fig. 1. Example of the volume-angle relationship for a braided cylinder. The inner volume increases upon pressurization, with θ and axial length increasing when $\theta < \theta^*$ ($A \rightarrow B$, extensor behavior) or decreasing when $\theta > \theta^*$ ($C \rightarrow D$, contractor behavior). For $\theta = \theta^*$, the inner volume has its maximum value and further pressurization causes no volume increment.

Historically, the mechanical response of McKibben actuators has been quantified by adopting two opposite approaches. On one hand, by approximating the mesh as a cylinder [1], we can derive a simple formula for the axial force necessary to balance a given pressurization by applying the Principle of Virtual Work (PVW). Further simplified models based on force or energy balance can be found in [3, 4] and in the many references cited therein. While some key features are captured, these modeling approaches are too simplistic to reproduce the behavior of braided meshes in a broad range of operating conditions. On the other hand, the Finite Elements Method (FEM) has been employed, describing each fiber as an individual beam linked together through boundary conditions [2, 5, 6, 7]. These simulations are indeed accurate, yet computationally expensive, and do not reveal the inner working principles of these structures.

In this paper, we define a physically insightful, computationally efficient framework to study the mechanical behavior of McKibben artificial muscles. Under the assumption of axisymmetric deformations, we derive a coarse-grained model by assuming that the kinematics of the virtual envelope surface, *i.e.*, the surface of revolution on which the centerlines of all fibers lie, resolves the one of the whole structure, both in the initial and deformed configurations. More technically, the core hypothesis allowing us to relate fiber and

[1]Jacopo Quaglierini is with The BioRobotics Institute, Scuola Superiore Sant'Anna, 56127 Pisa, Italy j.quaglierini@santannapisa.it

[2]Marino Arroyo is with LaCàN, Universitat Politècnica de Catalunya-BarcelonaTech, Centre Internacional de Mètodes Numèrics en Enginyeria (CIMNE), 08034 Barcelona, Institute for Bioengineering of Catalonia (IBEC), The Barcelona Institute for Science and Technology (BIST), 08028 Barcelona, Spain marino.arroyo@upc.edu

[3]Antonio DeSimone is with The BioRobotics Institute, Scuola Superiore Sant'Anna, 56127 Pisa, and SISSA, 34136 Trieste, Italy desimone@sissa.it, a.desimone@santannapisa.it

surface kinematics is that the Darboux frame of their center-lines coincides point-wise with the frame of directors during deformation, see Figure 2. As a consequence, the behavior of the mesh depends only on the angle $\theta(v)$ that the fibers form with the parallels of the envelope surface along its axis.

We then simulate the behavior of a McKibben artificial muscle, schematized as a braided mesh mechanically in parallel with an inner chamber, and compare our results with those obtained in Hassan et al. [2] who use a richer model, that however employs many more degrees of freedom. To give an idea of the gap in complexity, we need to solve a single ODE on 120 nodes, whereas a full 3D model based on FEM for rods presents, for each element, 3 unknown functions of 3 spatial variables, one for each component of the position field; the computational model in Hassan et al. uses 13,048 and 14,728 rod elements to simulate an extensor and contractor behavior, respectively.

Simulations show that, in a typical McKibben artificial muscle, loads are sustained mostly by the braided mesh, whereas the major part of the external work done on the structure is stored as elastic energy by the inner chamber. This fact explains why analytical formulas based on PVW (in which the presence of the chamber is not considered and the elastic energy stored by the mesh is neglected) can be so effective at predicting the behavior of McKibben actuators, as shown in Section III-B.

The remainder of this paper is organized as follows. In Section II, we present the mathematical framework of our model. In Section III, we present our main findings on McKibben actuators and compare numerical simulations with results found in literature. In Section IV, we discuss their implications and outline possible directions for future work.

II. Mathematical model and numerical implementation

We consider a McKibben actuator formed by an inner chamber and an external cylindrical braided mesh. The mesh has initial radius R_0, initial height H_0, and it is composed of N identical, inextensible, helical fibers; these fibers are organized in pairs of opposite chirality and share the same helical axis, as shown in Fig. 2. In the reference configuration, which we assume to be stress-free, right-handed helices form a positive angle $\theta_0 \in (0\,,\,\pi/2)$ with the parallels of the cylinder (braiding angle), while left-handed ones form an angle equal to $-\theta_0$, see inset in Fig. 2.

We describe the kinematics of the envelope surface, *i.e.*, the surface of revolution on which the center-lines of all fibers lie, in terms of the current braiding angle θ, that is, the angle that right-handed fibers form with the parallels of the mesh in the deformed configuration. Fibers are modeled as Kirchhoff rods with elastic energy expressed in terms of their strains [8]; we then further simplify our model by assuming that one of the directors of the cross section is always parallel to the normal to the envelope surface. Mathematically, this is equivalent to making the ansatz that the frame of directors of each fiber coincides with the Darboux frame of the envelope surface. Therefore, the elastic energy of fibers, through their strains, is a function of θ alone. As shown in Section III, the

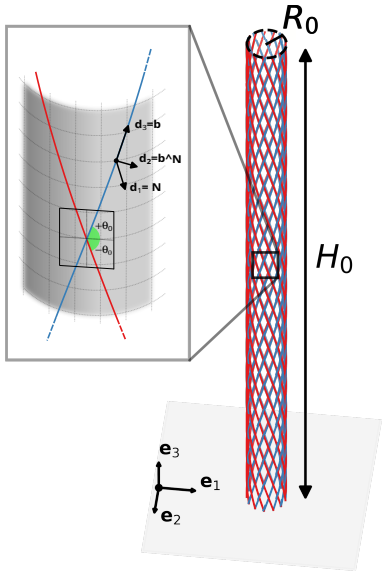

Fig. 2. Sketch of the initial configuration of the mesh of a McKibben actuator, with initial braiding angle θ_0. The inset shows the directors frame defined by the geometry of the envelope surface (see Section II-C).

results obtained using this simplifying assumption are still in good agreement with experiments in Hassan et al..

We then model the inner chamber as an incompressible rubber balloon, and we assume that the envelope surface of the braided mesh and the inner surface of the balloon coincide. The key idea is to model the actuator as the coupling in parallel of the braided mesh with the inflatable balloon contained by it. In this way, the overall internal energy of the structure is the sum of their individual ones.

A. Geometry and kinematics of the envelope surface

Let $\{\boldsymbol{e}_1, \boldsymbol{e}_2, \boldsymbol{e}_3\}$ be the global Cartesian reference frame, with $\boldsymbol{e}_3$ along the axis of the mesh. We assume no sliding between fibers; since fibers are mechanically equivalent and both right-handed and left-handed ones are present, the mesh does not rotate around $\boldsymbol{e}_3$ when subjected to axisymmetric loads. Thus, axisymmetric deformations of the envelope surface are parametrized by

$$\boldsymbol{\chi}(u,v) = \left(r(v)\cos\left(\frac{u}{R_0}\right),\, r(v)\sin\left(\frac{u}{R_0}\right),\, z(v)\right), \qquad (1)$$

where $u \in [0, 2\pi R_0]$, $v \in [0, H_0]$, are the circumferential and axial coordinates in the initial configuration, and r, z are the distance from the axis and the current axial coordinate. The differential $\mathrm{D}\boldsymbol{\chi}$ is computed as

$$\mathrm{D}\boldsymbol{\chi} = \left[\boldsymbol{\chi}_{,u},\, \boldsymbol{\chi}_{,v}\right], \quad \boldsymbol{\chi}_{,u} = \left(-\frac{r}{R_0}\sin\left(\frac{u}{R_0}\right),\, \frac{r}{R_0}\cos\left(\frac{u}{R_0}\right),\, 0\right), \quad (2)$$

$$\boldsymbol{\chi}_{,v} = \left(r_{,v}\cos\left(\frac{u}{R_0}\right),\, r_{,v}\sin\left(\frac{u}{R_0}\right),\, z_{,v}\right), \qquad (3)$$

where $(\cdot)_{,x}$ means derivative $\partial/\partial x$. The field of unit vectors normal to the surface $\boldsymbol{N} = (\boldsymbol{\chi}_{,u} \wedge \boldsymbol{\chi}_{,v})/\|\boldsymbol{\chi}_{,u} \wedge \boldsymbol{\chi}_{,v}\|$ is given by

$$\boldsymbol{N} = \frac{1}{\sqrt{r_{,v}^2 + z_{,v}^2}}\left(z_{,v}\cos\left(\frac{u}{R_0}\right),\, z_{,v}\sin\left(\frac{u}{R_0}\right),\, -r_{,v}\right). \qquad (4)$$

The coefficients of first and second fundamental forms are

$$E = \left(\frac{r}{R_0}\right)^2, \quad F = 0, \quad G = (r_{,v})^2 + (z_{,v})^2, \tag{5}$$

$$e = -\frac{r z_{,v}}{R_0^2\sqrt{G}}, \quad f = 0, \quad g = \frac{r_{,vv}z_{,v} - r_{,v}z_{,vv}}{\sqrt{G}}. \tag{6}$$

B. Imposing the inextensibility of fibers

Since the problem is axisymmetric and fibers are mechanically equivalent, each fiber will have the same elastic energy. Therefore, in the following we can focus only on the right-handed fibers without any loss of generality. We parametrize the center-line of a generic fiber in the u, v plane as

$$C(t) = \left((u_0 + t\cos(\theta_0))_{\mathrm{mod}(2\pi R_0)},\, t\sin(\theta_0)\right), \tag{7}$$

where $t \in [0\,,\, H_0 \sin^{-1}(\theta_0)]$ is the arc-length of the curve. The image of $C(t)$ on the envelope surface has tangent vector

$$\boldsymbol{b} := \boldsymbol{\chi}_{,t}(C(t)) = \cos(\theta_0)\boldsymbol{\chi}_{,u} + \sin(\theta_0)\boldsymbol{\chi}_{,v}, \tag{8}$$

and from the definition of θ we have

$$\boldsymbol{b}\cdot\boldsymbol{\chi}_{,u} = \|\boldsymbol{b}\|\sqrt{E}\cos(\theta_0) = \cos(\theta). \tag{9}$$

By imposing the inextensibility of fibers, *i.e.*,

$$\|\boldsymbol{b}\| = E\cos^2(\theta_0) + G\sin^2(\theta_0) = 1, \tag{10}$$

it is easy to show that

$$r = \frac{R_0}{\cos(\theta_0)}\cos(\theta), \tag{11}$$

$$z_{,v} = \frac{\sin(\theta)}{\sin(\theta_0)}\sqrt{1 - R_0^2\tan^2(\theta_0)\theta_{,v}^2}. \tag{12}$$

C. Fibers as elastic Kirchhoff rods

Fibers are modeled as elastic Kirchhoff rods, endowed with a positive orthonormal frame of directors $\{\boldsymbol{d}_1, \boldsymbol{d}_2, \boldsymbol{d}_3\}$. For a generic fiber, at each point along its center-line we can attach the corresponding Darboux frame, defined on the envelope surface as $\{\boldsymbol{b}, (\boldsymbol{b}\wedge\boldsymbol{N}), \boldsymbol{N}\}$. According to the Kirchhoff hypothesis, $\boldsymbol{d}_3$ coincides with the tangent vector $\boldsymbol{b}$. We assume, in addition, that one of the directors coincides with the normal vector, namely $\boldsymbol{d}_1 = \boldsymbol{N}$. Thus, the frame of directors coincides with the Darboux frame, *i.e.*,

$$\boldsymbol{d}_1(t) := \boldsymbol{N}, \quad \boldsymbol{d}_2(t) := \boldsymbol{b}\wedge\boldsymbol{N}, \quad \boldsymbol{d}_3(t) := \boldsymbol{b}. \tag{13}$$

Through some tedious yet straightforward manipulations, we can compute the vector of strains $\boldsymbol{u} = (u_1, u_2, u_3)^{\mathrm{T}}$ as [8]

$$u_1 = \boldsymbol{d}_{2,t}\cdot\boldsymbol{d}_3 = 2\sin(\theta_0)\theta_{,v}, \tag{14}$$

$$u_2 = \boldsymbol{d}_{3,t}\cdot\boldsymbol{d}_1 = -\frac{\cos(\theta_0)\sin(\theta_0)}{R_0\tan(\theta)}z_{,v} - R_0\tan(\theta_0)\sin^2(\theta)\frac{\theta_{,vv}}{z_{,v}}, \tag{15}$$

$$u_3 = \boldsymbol{d}_{1,t}\cdot\boldsymbol{d}_2 = \frac{\cos(\theta_0)\sin(\theta_0)}{R_0}z_{,v} - \frac{R_0\tan(\theta_0)}{2}\sin(2\theta)\frac{\theta_{,vv}}{z_{,v}}. \tag{16}$$

By substituting Eq. (12) in these expressions, we conclude that strains are functions of $\theta(v)$ alone, *i.e.*,

$$u_i \equiv u_i(\theta(v)), \quad i = 1, 2, 3. \tag{17}$$

Therefore, the initial geometry of the mesh and $\theta(v)$ fully describe the geometry of the deformed envelope surface, which in turn resolves the kinematics of the fibers. In the initial configuration ($\theta \equiv \theta_0$), strains are given by

$$u_{1\,0} = 0, \quad u_{2\,0} = -\frac{\cos^2(\theta_0)}{R_0}, \quad u_{3\,0} = \frac{\cos(\theta_0)\sin(\theta_0)}{R_0}. \tag{18}$$

D. Energetics of the mesh

We find the equilibrium configurations of the mesh by using the Principle of Virtual Work, which requires

$$\delta\boldsymbol{\mathcal{E}}(\theta;\, \delta\theta) = 0, \quad \forall\,\delta\theta, \tag{19}$$

where $\boldsymbol{\mathcal{E}}$ is the potential energy of the system given by the difference between internal energy and work done by external loads, and $\delta(\cdot)$ denotes a virtual variation. The internal energy of the system is the elastic energy of the mesh, *i.e.*, the one of a single fiber times their number,

$$\mathcal{E}_{\mathrm{el}} := \frac{N}{2\sin\theta_0}\int_0^{H_0}[B_1\,(u_1 - u_{1\,0})^2 + \\ + B_2\,(u_2 - u_{2\,0})^2 + B_3\,(u_3 - u_{3\,0})^2\,]\,\mathrm{d}v. \tag{20}$$

Here, B_1, B_2 represent the bending stiffnesses of fibers along $\boldsymbol{d}_1, \boldsymbol{d}_2$, and B_3 their torsional stiffness along $\boldsymbol{d}_3$. Compression can be achieved either by applying a given axial force F, in which case the work term $\mathcal{E}_{\mathrm{F}}$

$$\mathcal{E}_{\mathrm{F}} = F\left(\int_0^{H_0} z_{,v}\,\mathrm{d}v - H_0\right) \tag{21}$$

must be subtracted from $\mathcal{E}_{\mathrm{el}}$, or by imposing the height of the mesh to be equal to h_{target}, in which case we subtract from $\mathcal{E}_{\mathrm{el}}$ the term $\mathcal{E}_{\mathrm{h}}$

$$\mathcal{E}_{\mathrm{h}} = \lambda_{\mathrm{h}}\left(\int_0^{H_0} z_{,v}\,\mathrm{d}v - h_{\mathrm{target}}\right), \tag{22}$$

where λ_{h} is a Lagrange multiplier.

E. Modeling of the inner chamber

We model the inner chamber as an incompressible hollow cylinder with initial radius R_0, initial height H_0 and initial thickness t_0. Since $t_0 << R_0, H_0$, stretches are approximately constant across the thickness. By assuming that the balloon is already in contact with the mesh and that there is no sliding between them, at contact points they share the same metric and are subjected to the same constraint of inextensibility along the fibers; by considering a "dense enough" mesh, we can extend this assumption to all points of the surface. Thus, in the basis $\{\boldsymbol{\chi}_{,u}, \boldsymbol{\chi}_{,v}, \boldsymbol{N}\}$ the metric tensor of the balloon is

$$\boldsymbol{C} = \begin{bmatrix} \lambda_1^2 & 0 & 0 \\ 0 & \lambda_2^2 & 0 \\ 0 & 0 & \lambda_3^2 \end{bmatrix} = \begin{bmatrix} E & 0 & 0 \\ 0 & G & 0 \\ 0 & 0 & (EG)^{-1} \end{bmatrix}, \tag{23}$$

where

$$\lambda_1 = \frac{\cos(\theta)}{\cos(\theta_0)}, \quad \lambda_2 = \frac{\sin(\theta)}{\sin(\theta_0)}, \quad \lambda_3 = \frac{\sin(2\theta_0)}{\sin(2\theta)} \tag{24}$$

are the principal stretches, with λ_3 obtained from the constraint of incompressibility ($\det(\boldsymbol{C}) = 1$). We describe the

elastic energy of the balloon by adopting an incompressible Mooney-Rivlin model, with energy density

$$\psi(\boldsymbol{C}) := c_1\,(I_1(\boldsymbol{C}) - 3) + c_2\,(I_2(\boldsymbol{C}) - 3) = \\ = -3(c_1 + c_2) + \sum_{i=1}^{3} c_1\lambda_i^2 + c_2\lambda_i^{-2}\,, \qquad (25)$$

where I_1, I_2 are the first two principal invariants of $\boldsymbol{C}$, and c_1, c_2 are material parameters. Under the hypothesis of constant stretches across thickness, the elastic energy of the balloon simplifies to

$$\mathcal{E}_{\text{balloon}} := A_0 \int_0^{H_0} \psi(\boldsymbol{C}(v))\,\mathrm{d}v\,, \quad A_0 := \pi t_0(t_0 + 2R_0)\,, \qquad (26)$$

where A_0 is the area of any annular cross-section of the initial cylinder. The work done by a constant internal pressure P is

$$\mathcal{E}_{\text{P}} := P(V - V_0) = \pi P\left(\int_0^{H_0} r^2 z_{,v}\,\mathrm{d}v - H_0 R_0^2\right), \qquad (27)$$

where V_0, V are inner volumes in the reference and current configuration, respectively. The total potential energy reads

$$\mathcal{E} = \mathcal{E}_{\text{el}} + \mathcal{E}_{\text{balloon}} - \mathcal{E}_{\text{c}} - \mathcal{E}_{\text{P}}\,, \qquad (28)$$

where $\mathcal{E}_{\text{c}}$ is either equal to $\mathcal{E}_{\text{F}}$ or $\mathcal{E}_{\text{h}}$ (see Eqs. (21),(22)).

F. Numerical implementation

We implemented the previously described mathematical model with a MATLAB® custom code, where we minimize Eq. (22) with respect to $\theta(v)$, discretized into 43 points through a clamped cubic B-spline; a Gauss-Legendre quadrature of order 3 is adopted, obtaining 120 Gauss nodes. The cubic spline ensures a smooth second derivative of θ, and using Gauss nodes as discretization points allows us to have a good approximation of the integrals in the energy functional.

III. Results

To validate the proposed model against experimental evidence, we compare our results with those of [2], who investigated the mechanical response of a McKibben actuator with a FEM model and compared it with experimental results, as well as analytical approximated formulas obtained through the Principle of Virtual Work (PVW). The actuator considered has initial height $H_0 = 85$ mm, initial radius $R_0 = 12.5$ mm, and initial braiding angle $\theta_0 = 37°$, close to the "magic angle" θ^*. Four cases were investigated:

1) Quasi-static Isometric tests
   a) the McKibben actuator is pre-stretched and kept at a fixed length of 115 mm; then it is subjected to an internal pressure increasing from 0 to 1 bar, and the axial loads are recorded (compressor behavior);
   b) the McKibben actuator is pre-compressed and kept at a fixed length of 55 mm; then it is subjected to an internal pressure increasing from 0 to 1 bar, and the axial loads are recorded (extensor behavior);
2) Quasi-static Isobaric relaxation
   (c) the McKibben actuator is pre-stretched at a length of 115 mm; at this nominal position, it is gradually pressurized from 0 to 1 bar, and then kept at constant pressure. The top end-fitting is allowed to relax until the axial load vanishes, and the corresponding displacement is recorded (compressor behavior);
   (d) the McKibben actuator is pre-compressed at a length of 55 mm; at this nominal position, it is gradually pressurized from 0 to 1 bar, and then kept at constant pressure. The top end-fitting is allowed to relax until the axial load vanishes, and the corresponding displacement is recorded (extensor behavior).

The number of fibers N, bending and torsional stiffnesses B_1, B_2, B_3, and material parameters c_1, c_2, are set equal to the ones found in [2].

For cases a), b), we also report analytical profiles of the force-pressure relationship, obtained by applying PVW to an infinitesimal cylinder at the center of the deformed mesh, derived in Section III-A. In this way, we extend the argument used in [1] for finite cylinders to non-cylindrical geometries.

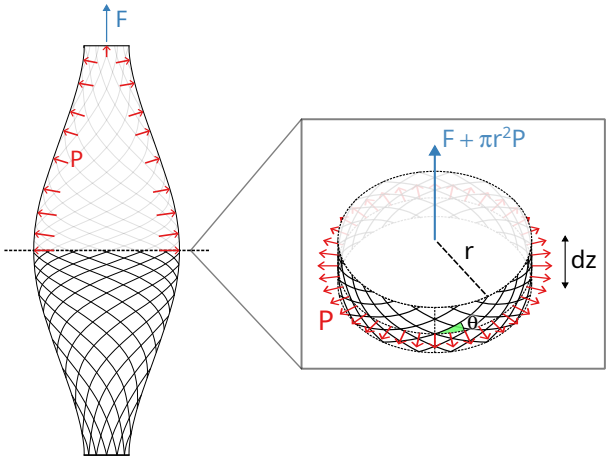

Fig. 3. Sketch of the application of the PVW to an infinitesimal cylinder at the center of a mesh subjected to an axial force and internal pressure.

A. Analytical formulas from the Principle of Virtual Work

Considering a generic mesh in equilibrium under an axial force F and internal pressure P, we focus on an infinitesimal cylinder at its center, with radius r, height $\mathrm{d}z$, and braiding angle θ, see Fig. 3. Assuming that the mesh stores no elastic energy, the PVW on the infinitesimal cylinder states that

$$2\pi r\mathrm{d}z P\delta r + \left(F + \pi r^2 P\right)\delta(\mathrm{d}z) = 0\,. \qquad (29)$$

Kinematic constraints from Eqs. (11),(12) become

$$r = \frac{R_0}{\cos(\theta_0)}\cos(\theta)\,, \quad \mathrm{d}z = \frac{\mathrm{d}z_0}{\sin(\theta_0)}\sin(\theta)\,, \qquad (30)$$

where $\mathrm{d}z_0$ is the height of the infinitesimal cylinder in the reference straight configuration. Substituting them in Eq. (29) we obtain

$$F = \frac{\pi R_0^2}{\cos^2(\theta_0)}\left(3\sin^2(\theta) - 1\right)P\,. \qquad (31)$$

We use Eq. (31) for cases a), b) with θ equal to the braiding angle at the center of the mesh after pre-stretch

or pre-compression but before pressurization. Eq. (31) is a good approximation for the force-pressure relationship of a McKibben actuator provided that the following three conditions are met:

1) the mesh stores no elastic energy but accurately imposes the kinematic constraints in Eqs. (11),(12);
2) loads on the structure are sustained entirely by the mesh;
3) upon pressurization, the angle θ at the center of the mesh does not change.

B. Comparison with Hassan et al.

Figure 4 compares the force-pressure or displacement-pressure profiles obtained through our model with the results reported in [2], as well as the analytical approximations for cases a), b) following Eq. (31), showing that there is a good matching between analytical and numerical curves. In fact, simulations highlight that the value of θ at the center of the mesh does not change much with applied pressure, and that loads are sustained mostly by the braided mesh.

Considering the infinitesimal cylinder at the center of the mesh, since the balloon absorbs essentially all the external work done on the structure, see Fig. 5, the working hypothesis of no elastic energy stored in the braided mesh is verified. At the same time, since the load fraction transmitted by the balloon is negligible, the axial force exerted by the entire structure matches the one exerted by the mesh as predicted by PVW. Therefore, these results clarify why the analytical approach based on PVW yields — in this case — accurate results in spite of the presence of the balloon and the fact that deformed shapes are not cylinders.

For what regards the comparison with [2], there are some small discrepancies in cases b), c), and more pronounced ones in cases a) and especially d). These can be attributed to the inherent differences with respect to both their FE model and experimental prototype. Indeed:

1) We do not model the interlacing of fibers;
2) We do not ignore the initial stresses of the structure;
3) Our internal chamber follows a cylindrical profile, not a bellows-like one as in [2];
4) Our internal chamber is in contact with the mesh from the beginning of the experiment, and the two sub-structures have the same initial length and diameter;
5) We do not take sliding of fibers into account.

Finally, we note that the simplified model embodied in Eq. (31) is not always a suitable approximation. For instance, if fibers are thicker or stiffer, then besides their effect in imposing the kinematic constraints through their inextensibility, bending and torsional energy should play a role. Since these effects are accounted for in our theory but not in the analytical formula (31), differences are to be expected. Considering case b), Figure 6 compares these two models for a McKibben actuator with mesh fibers a hundred times stiffer than the ones in [2]. Now, Eq.(31) leads to noticeable errors, which from the energy density plots can be ascribed to the elastic energy of fibers.

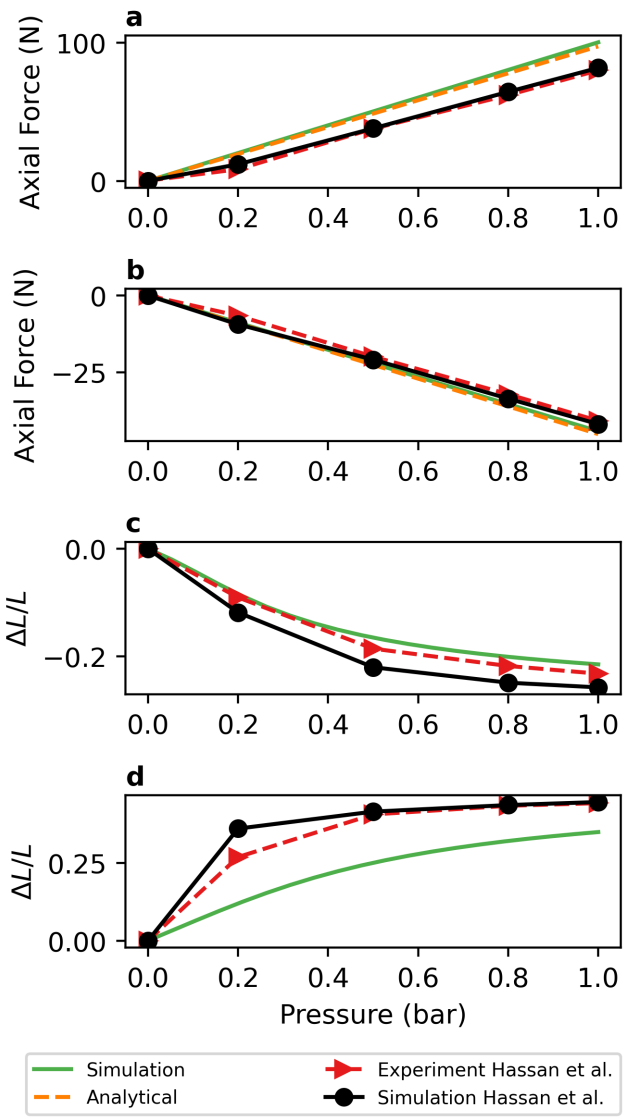

Fig. 4. a,b) Comparison between the force-pressure curve obtained by simulating case a,b) through our model and the one presented in [2]. A force profile obtained by applying PVW is reported as well. c,d) Comparison between the strain-pressure curve obtained by simulating case c,d) through our model and the one presented in [2]. Here, L is the length of the actuator before pressurization, 115 mm for case c) and 55 mm for case d), and ΔL represents their variations.

IV. Discussion and Conclusions

Our results highlight a clear separation of roles between outer braided mesh and inner chamber in McKibben actuators. The braided mesh sustains loads and imposes the kinematic constraints of the structure through fiber inextensibility, whereas the external work done on the structure is stored as elastic energy for the major part by the inner chamber. This separation of roles, *i.e.*, the braided mesh sustains loads and restricts kinematics without storing energy, while the chamber stores the external work without transmitting forces, clarifies why the simplified analytical formulas for the force-pressure relationship, based on Principle of Virtual Work,

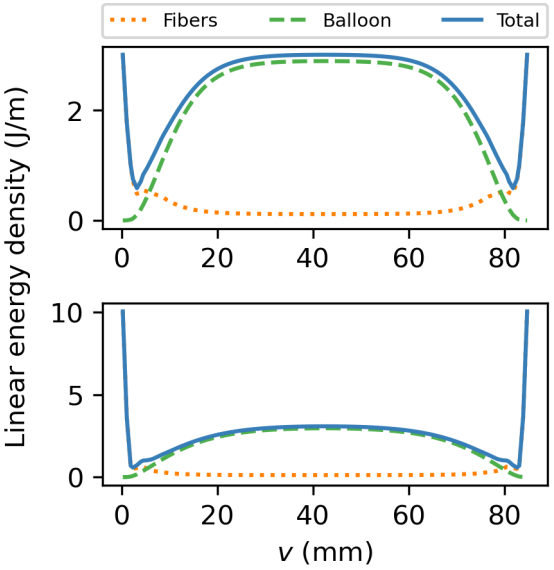

Fig. 5. Comparison between the elastic energy density of the mesh and the balloon during the blocked-force test of case a) in the initial (top) and final configuration (bottom) . At the center of the mesh, the energy density of the fibers is negligible with respect to the one of the balloon. This shows that, considering the infinitesimal cylinder at the center of the mesh, external work is stored as elastic energy almost entirely by the balloon.

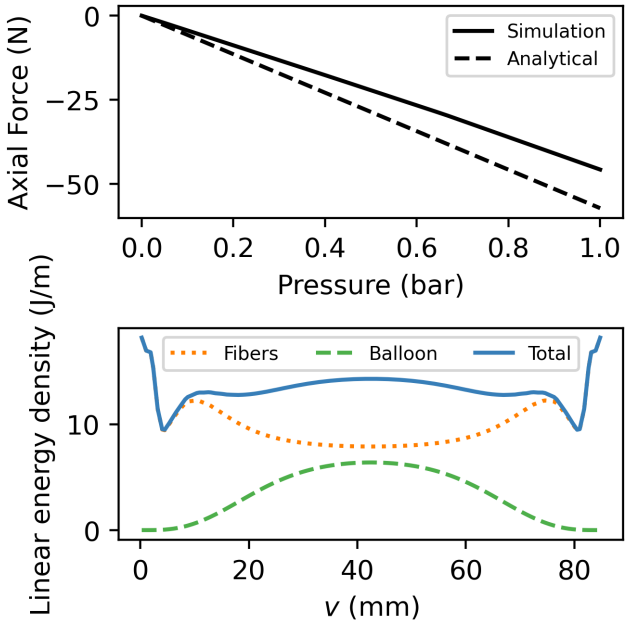

Fig. 6. On the top, comparison between numerical and analytical force-pressure profiles for a McKibben actuator identical to the one investigated by [2], except that the Young's modulus of its fibers is a hundred times larger. On the bottom, the elastic energy density of the mesh after pressurization.

provide a good approximation as explained in Section III-B.

Our model shows higher accuracy than currently available geometric models (see Fig. 6). In fact, our results show good matching with those obtained from more complex FEM models, while requiring a fraction of their computational cost, making our model a promising tool for design optimization.

In future work, we plan to extend our formulation to capture effects not yet included in our model such as friction, sliding, and interweaving of fibers. Also, it would be interesting to choose different models for the elastic energy of fibers, with energy densities growing with respect to the strains faster than quadratically.

Acknowledgments

We thank T. Hassan Shah for sharing experimental and computational data from ref. [2]. J.Q. and A.D.S. acknowledge the support of the Italian Ministry of University and Research (PRIN-2020PFCXPE) and of the European Union's Horizon 2020 and Horizon Europe Research and Innovation Programmes (I-Seed GA-101017940, MAPWORMS GA-101046846). A.D.S. is a member of the INdAM Research Group GNFM. M.A. acknowledges the support of the Generalitat de Catalunya (AGAUR: 2017-SGR-1278, "ICREA Academia" award to M.A.), the European Research Council (CoG-681434 to M.A.). IBEC and CIMNE are recipients of a Severo Ochoa Award of Excellence from the MINECO.

References

[1] B. Tondu, "Modelling of the McKibben artificial muscle: A review," *Journal of Intelligent Material Systems and Structures*, vol. 23, no. 3, pp. 225–253, 2012.

[2] T. Hassan, M. Cianchetti, M. Moatamedi, B. Mazzolai, C. Laschi, and P. Dario, "Finite-element modeling and design of a pneumatic braided muscle actuator with multifunctional capabilities," *IEEE/ASME Transactions on Mechatronics*, vol. 24, no. 1, pp. 109–119, 2018.

[3] B. Kalita, A. Leonessa, and S. K. Dwivedy, "A review on the development of pneumatic artificial muscle actuators: Force model and application," in *Actuators*, vol. 11, no. 10. MDPI, 2022, p. 288.

[4] J. Garbulinski, S. C. Balasankula, and N. M. Wereley, "Characterization and analysis of extensile fluidic artificial muscles," in *Actuators*, vol. 10, no. 2. MDPI, 2021, p. 26.

[5] G. Olson, S. Pellegrino, J. Banik, and J. Costantine, "Deployable helical antennas for cubesats," in *54th AIAA/ASME/ASCE/AHS/ASC Structures, Structural Dynamics, and Materials Conference*, 2013, p. 1671.

[6] J. Quaglierini, A. Lucantonio, and A. DeSimone, "Mechanics of tubular helical assemblies: ensemble response to axial compression and extension," *Acta Mechanica Sinica*, vol. 37, no. 2, pp. 173–186, 2021.

[7] M. G. Antonelli, P. Beomonte Zobel, F. Durante, and T. Raparelli, "Numerical modelling and experimental validation of a mckibben pneumatic muscle actuator," *Journal of Intelligent Material Systems and Structures*, vol. 28, no. 19, pp. 2737–2748, 2017.

[8] S. S. Antman, "Problems in nonlinear elasticity," *Nonlinear Problems of Elasticity*, pp. 513–584, 2005.